


## Research Article

# Experimental Investigation of the Continuous Transition of Flame-Spreading near the Blow-Off Limit

K. Komizu <sup>1</sup>, Y. Saito,<sup>2</sup> A. Tsuji,<sup>1</sup> and H. Nagata<sup>3</sup>

<sup>1</sup>Faculty of Engineering, Hokkaido University, Sapporo 060-8628, Japan

<sup>2</sup>Department of Aerospace Engineering, Tohoku University, Sendai 980-8579, Japan

<sup>3</sup>Graduate School of Engineering, Hokkaido University, Sapporo 060-8628, Japan

Correspondence should be addressed to K. Komizu; kkbbaseball0808@gmail.com

Received 1 November 2019; Accepted 6 January 2020; Published 19 February 2020

Academic Editor: Bruce Chehroudi

Copyright © 2020 K. Komizu et al. This is an open access article distributed under the Creative Commons Attribution License, which permits unrestricted use, distribution, and reproduction in any medium, provided the original work is properly cited.

This study investigates the continuous transition from flame-spreading to stabilized combustion near the blow-off limit in opposed forced flow by using expanding solid fuel duct that makes distribution of oxidizer velocity in the axial direction. The stabilized combustion is a diffusion flame that appears in the Axial-Injection End-Burning Hybrid Rocket. The boundary between flame-spreading and stabilized combustion has not been investigated in detail. Polymethyl methacrylate (PMMA) rectangular ducts were used as a fuel, and gaseous oxygen was used as an oxidizer. All firing tests were conducted at atmospheric pressure. The diffusion flame traveled in the opposed-flow field where the oxidizer velocity increases continuously in the upstream direction. The combustion mode changed when oxidizer velocity at the flame tip exceeded a certain value. The oxidizer velocity used in this experiment ranges from 0.6 to 32.8 m/s. Experimental results show that a threshold oxidizer velocity of the transition can be determined. In this study, the threshold velocity was 26.4 m/s.

## 1. Introduction

Flame spread over combustible solids into an opposed flow of oxidizer has been investigated by various researchers [1]. In an opposed flow of a sufficiently large velocity (e.g., 20 m/s), the diffusion flame spreading on the combustible flat plate extinguishes or cannot be ignited because the residence time for the gas mixture in the flow is insufficient. In a narrow fuel duct, however, Hashimoto et al. [2] observed that the diffusion flame does not extinguish when the opposed oxidizer flow velocity is sufficiently high, and slowly moves toward the upstream direction while widening the fuel. This combustion mode is called stabilized combustion (Figure 1). In this combustion mode, the flame-traveling velocity (or flame spreading rate) is the velocity at which the flame widens the duct by fuel consumption. Therefore, the flame spreading rate ( $V_f$ ) is significantly low compared with flame-spreading combustion, e.g.,  $V_f = 0.7$  mm/s for stabilized combustion and  $V_f = 5.5$  mm/s for flame spreading combustion under the conditions of atmospheric pressure, PMMA of the inner

diameter of 2 mm, and pure oxygen [2]. Thus, the combustion mode can be distinguished by the flame spreading velocity and/or fuel regression shape.

The boundary between the flame-spreading combustion and the stabilized combustion has been investigated. Hashimoto et al. showed that friction velocity at the boundary between the two combustion modes is constant for turbulent flow [3]. As for laminar flow, Matsuoka et al. [4] showed that friction velocity at the boundary is constant. They also indicated that the constant friction velocity results in the constant critical Damköhler number (Da) at the boundary, and thus, the phenomenon of the transition to stabilized combustion is physically identical to the phenomenon of blow-off.

Stabilized combustion has been used for a new type of hybrid rocket. We “have been” investigating the hybrid rocket, Axial-Injection End-Burning Hybrid Rocket (EBHR), which uses a cylindrical fuel with an array of many small ports running in the axial direction, through which oxidizer gas flows [5–7]. Stabilized combustion is kept at

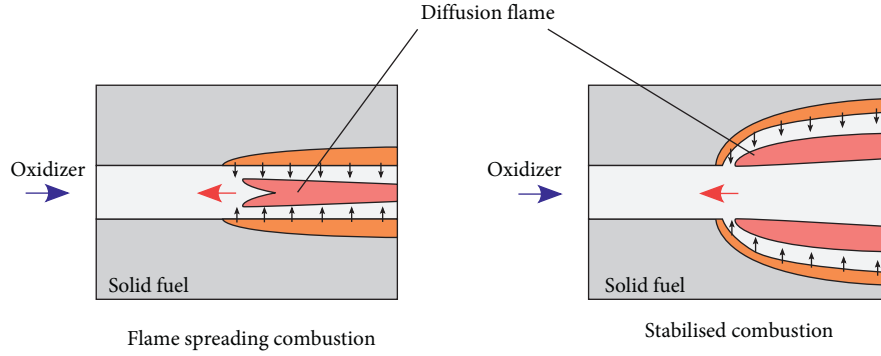


FIGURE 1: Schematic representation of combustion modes in a narrow fuel duct.

each port exit. The fuel regresses due to heat input from these diffusion flames of the fuel end face (End-Burning). The researches reported that, in some cases, End-Burning could not persist because stabilized combustion mode suddenly changed to flame spreading combustion mode, possibly due to the influence of port accuracy. It is called the backfiring problem. Therefore, from the viewpoint of the development of EBHR, the study about the transition of stabilized combustion is important and interesting.

The influence of the oxidizer flow velocity in the port on each combustion mode has been investigated by conducting combustion experiments in which the oxidizer flow velocity is constant in each experiment [2–4]. Because the condition for appearing stabilized combustion was focused on in the abovementioned tests, the relation between the flame spreading rate and the oxidizer flow rate could only be investigated discretely, and the transition from flame spreading combustion to stabilized combustion modes has not been examined in detail. Therefore, in this research, we focused on the transition of flame spreading near the blow-off limit. To observe the transition from flame-spreading combustion to the stabilized combustion, the expanding flow duct whose flow velocity increases continuously was used.

## 2. Materials and Methods

**2.1. Fuel (Test Sample).** A fuel duct was designed to produce an opposed flow configuration where the oxidizer velocity increases continuously in the upstream direction. The fuel shape is shown in Figure 2, and its dimensions are specified in Table 1. The width of the fuel ducts was uniform in the axial direction, while the height of the ducts increased at an angle of 1 degree, resulting in an appropriate axial oxidizer velocity distribution. Because of the duct shape, the oxidizer flow velocity decreases as it flows downstream. Since the flame is ignited downstream, the oxidizer flow velocity at the tip of the flame increases as spreading upstream. An expanding flow path was created by bonding a flat plate with another plate which has an expanding groove. Transparent PMMA was used as fuel to measure the flame spreading rate by using a digital camera. In this study, to conduct experiments under the thermally thick condition, the vertical preheated length  $L_{sy} \approx \sqrt{\alpha_s \alpha_g / V_f V_o}$  [8] in the solid phase

was predicted from the experimental results which were conducted by Fenandez-Pello et al. [9]. When the fuel thickness is larger than  $L_{sy}$ , the fuel is thermally thick. Since the maximum value of  $L_{sy}$  was 1.0 mm, we employed the thickness of at least 10 mm. The fuels were thermally thick under all observed velocity of flame propagation ( $V_f$ ).

Figure 3 schematically shows a test sample. The fuel connects to the gas inlet part made of stainless steel with epoxy resin. The gas inlet part connects to a gas supply line. From the fuel shape and mass flow rate, it is possible to calculate the oxidizer flow velocity distribution in the duct by using the following equation based on the continuity equation:

$$V_o = \frac{Q}{A} = \frac{\dot{m}_o RT}{Pb\{h_i + (L - x)\tan 1^\circ\}} \quad (1)$$

where  $V_o$  (m/s) is oxidizer flow velocity,  $Q$  (m<sup>3</sup>/s) is volume flow rate,  $A$  (m<sup>2</sup>) is cross sectional area,  $\dot{m}_o$  (kg/s) is mass flow rate,  $R$  (J/kg/K) is gas constant,  $T$  (K) is temperature,  $P$  (Pa) is pressure,  $b$  (m) is a duct width,  $h_i$  (m) is an initial height of duct,  $L$  (m) is a duct length, and  $x$  (m) is a position of flame tip.

**2.2. Experimental Setup.** Figure 4 shows a schematic of the experimental apparatus. It mainly consists of an oxygen tank, a nitrogen tank, and the test sample. Pure oxygen was used as an oxidizer and nitrogen was used for a purge. There are 2 lines to supply gaseous oxygen and nitrogen. The oxygen line has a ball valve, needle valve, and nonreturn valve for flow/nonflow control, controlling gas flow rate, and preventing return flow, respectively. The nitrogen line has only a ball valve for flow/nonflow control. A mass flow meter measured the oxygen mass flow rate, and a pressure sensor measured the pressure at upstream of the fuel duct. The measured data are transmitted to the logger and stored. Table 2 shows the instruments used for the measurement and their accuracy.

The oxidizer mass flow rate was adjusted and choked by a needle valve. While feeding oxygen into the test sample, the fuel duct was ignited downstream by an ignited incense or heated nichrome wire. Then, the flame spreads into the fuel duct. A digital camera recorded the progress of the flame inside the fuel. When the flame reached the inlet, the oxygen

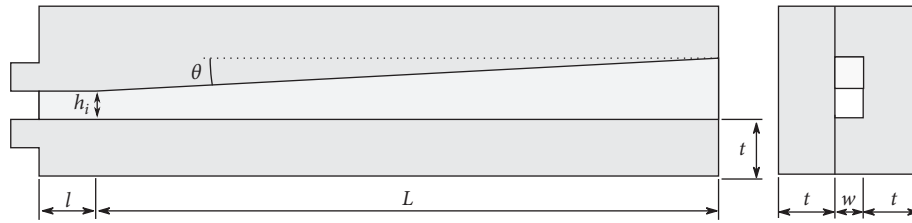


FIGURE 2: Fuel shape.

TABLE 1: Detail fuel shape.

Duct width (const.)	$w$	5	mm
Initial height	$h_i$	5	mm
Test section length	$L$	300	mm
	$l$	10	mm
Inclination	$\theta$	1	Degree
Thickness	$t$	10	mm

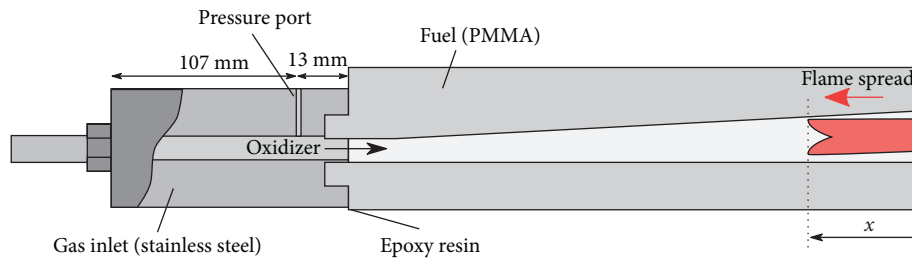


FIGURE 3: Test sample.

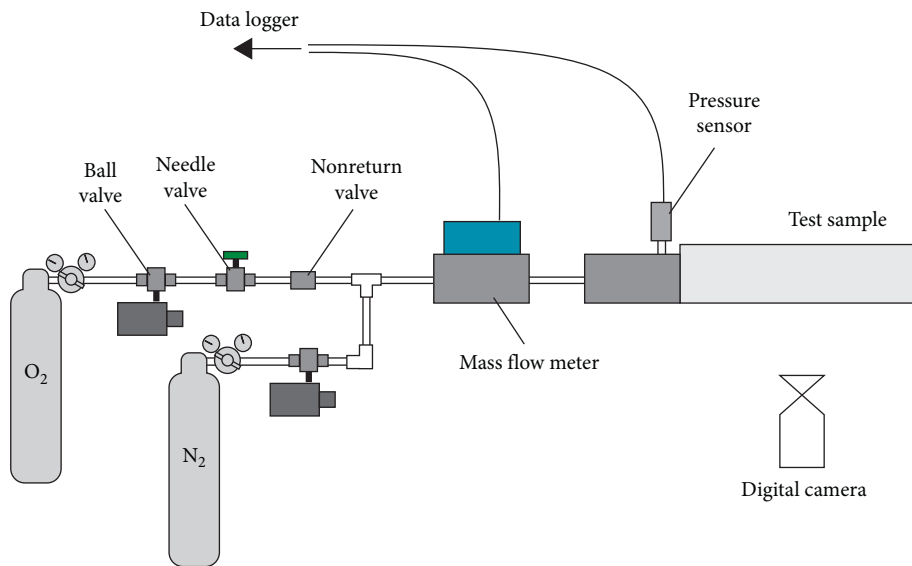


FIGURE 4: Experimental apparatus.

TABLE 2: Instruments and accuracy.

Instruments	Model number	Accuracy
Pressure sensor	PHB-A-2MP/KYOWA	$\pm 1.04$ kPa
Mass flow meter	CMS0500/azbil	$5 \leq Q < 50$ L/min: $\pm 1\%FS \pm 1$ digit $50 \leq Q < 500$ L/min: $\pm 3\% RD \pm 1$ digit
Maas flow meter	CMS0050/azbil	$0.5 \leq Q < 5$ L/min: $\pm 1\%FS \pm 1$ digi $5 \leq Q < 50$ L/min: $\pm 3\% RD \pm 1$ digit

was switched to nitrogen for a purge. All tests were conducted at atmospheric pressure.

### 3. Data Reduction

**3.1. Flame Spreading Rate and Oxygen Velocity.** Oxygen mass flow rate and pressure were measured during firing tests. The flame spreading rate was calculated by tracking the position history of the flame tip in the video by ImageJ. From the time history of the flame tip position, the mass flow rate, and the pressure, oxygen velocity at the flame tip was calculated by equation (1). The pressure at the flame tip was identified by the pressure at the pressure port because pressure drop from pressure port to the duct outlet calculated from equation (2) was less than 0.5 kPa (around 107 kPa at test condition). Since flame moves toward the upstream during a firing test, the actual pressure drop will be much less than 0.5 kPa. The resistance coefficient of the pipe was calculated by equation (3) for laminar flow and equation (4) for turbulent flow (Blasius resistance formula).

$$\Delta P = \int_0^L \lambda \frac{1}{D_e} \frac{\rho V_o^2}{2} dx, \quad (2)$$

$$\lambda = \frac{64}{Re}, \quad (3)$$

$$\lambda = 0.3164 Re^{-1/4}. \quad (4)$$

**3.2. Boundary Velocity.** To evaluate the boundary, the bulk velocity equation (1) gives was employed. The boundary condition between the two combustion modes has been investigated [3, 4]. The combustion mode depends upon

whether flow separation exists or not at the flame leading edge. If the boundary layer over the solid surface receives enough momentum from the core flow, the flow does not separate from the surface, and the flame cannot spread against the flow. Accordingly, the turbulent momentum transfer from the core flow to the boundary layer decides whether the flame can spread against the flow or not. Due to this finding, they found that friction velocity is an important indicator deciding whether the mode is flame spreading or stabilizing combustion. The following equation gives friction velocity for the turbulent regime:

$$u_{*,t} = 0.1989 V_o^{7/8} \left( \frac{\mu}{\rho d} \right)^{1/8}, \quad (5)$$

where  $V_o$  (m/s),  $\mu$  (Pa s),  $\rho$  (kg/m<sup>3</sup>), and  $d$  (m) are bulk velocity, viscosity, density of oxidiser, and port diameter. The boundary is expressed by a single value of the friction velocity regardless of other conditions [3]. Please note that the boundary expressed by a friction velocity is scale-independent. Near the transition point in this study, the Reynolds number was over 10,000, meaning that the flow was turbulent. By employing the friction velocity, we can use the result this paper provides to design EBHR at any scale. Accordingly, the discussion about the detailed velocity profile in the duct is not necessary. In this study, therefore, bulk velocity is used for boundary conditions.

**3.3. Error Bias.** The value of the oxidizer velocity has some error bias  $B_{V_o}$  because of the accuracy of instruments. In this study, the error bias  $B_{V_o}$  is determined by equation (6) using each error bias  $B_i$  of the instrument, which is summarised in Table 3.

$$B_{V_o} = \sqrt{\left( \frac{\partial V_o}{\partial \dot{m}_o} B_{\dot{m}_o} \right)^2 + \left( \frac{\partial V_o}{\partial P} B_P \right)^2 + \left( \frac{\partial V_o}{\partial b} B_b \right)^2 + \left( \frac{\partial V_o}{\partial h} B_h \right)^2 + \left( \frac{\partial V_o}{\partial L} B_L \right)^2 + \left( \frac{\partial V_o}{\partial x} B_x \right)^2}. \quad (6)$$

## 4. Results and Discussion

Several firing tests were conducted to observe the behavior near the blow-off limit. Figure 5 shows typical images of the flame. The images show that the flame spreading rate slowed down at around 25 s; the flame slowly moves while widening the duct. This means the combustion mode has transitioned from flame-spreading combustion to stabilized combustion. Accordingly, the transition between combustion modes was successfully observed.

Table 4 and Figure 6 summarize the results of the firing tests. In Figure 6, the horizontal axis represents the oxidizer flow velocity, and the vertical axis represents the flame spreading rate. The flame spreading rate changed as oxidizer flow velocity changed. The flame spreading rate increases with the flow velocity and then starts to decrease as the gas velocity increases. This trend qualitatively corresponds with

the combustion on the plate [9]. For the high oxidizer velocity region (around 26 m/s, near the blow-off limit),  $V_f-V_o$  relation is changed when the oxidizer velocity over a certain value. This velocity is transition velocity. The  $V_f-V_o$  relation near the blow-off limit became clear.

Figure 7 shows time histories of pressure and flame spreading rate in Test 6. The pressure marginally increased just after ignition and then decreased as the flame spreading rate decreased. When the flame spreading rate is fast, the flame increased the combustion area faster than it expanded combustion volume, so the pressure increased. For low flame spreading rate, however, the flame expanded the volume faster than it increased the area, so the pressure maintained constant. The pressure in tests 4–6 which were observed to have transition had the same tendency.

Figure 8 is a diagram focusing on a region where the flame spreading velocity is sufficiently low in Figure 6.

TABLE 3: Error bias of instrument.

	Item	Bias
$\dot{m}_o$	CMS500	3% of $\dot{m}_o$ + $2.2 \times 10^{-5}$ kg/s
$P$	PHB-A-2MP	1.04 kPa
$b$	Digital caliper	0.01 mm
$h$	Digital caliper	0.01 mm
$L$	Stainless scale	0.1 mm
$x$	ImageJ	Length per pixels (around 0.2 mm)

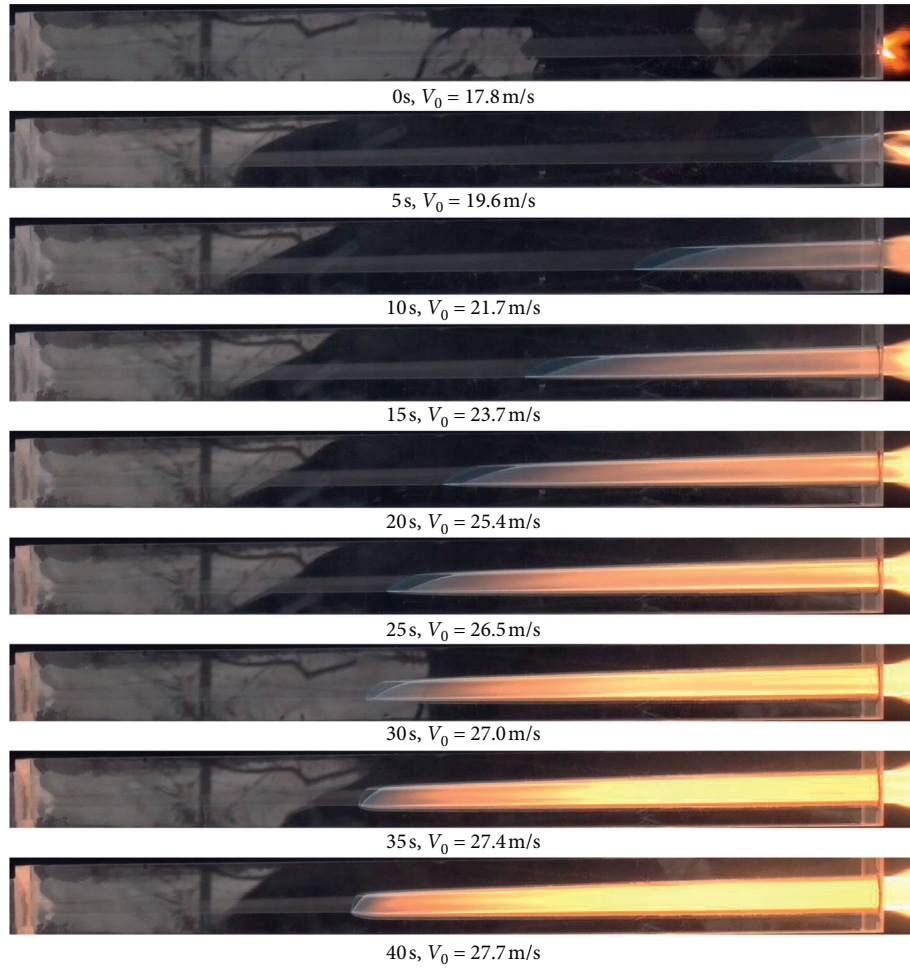


FIGURE 5: Typical images of the flame (Test 6).

TABLE 4: Firing results.

Test	$V_o$ range (m/s)	Firing results
01	0.6–1.1	Flame-spreading
02	1.8–3.6	Flame-spreading
03	11.8–20.3	Flame-spreading
04	18.0–29.1	Transition
05	16.5–31.7	Transition
06	18.5–32.8	Transition

When the oxidizer velocity exceeded around 26 m/s, flame spreading rate became much lower than before the flow rate exceeded the velocity and almost did not decelerate beyond  $V_f = 0.6$  mm/s. Therefore, the threshold oxidizer

velocity of the transition can be determined. Figure 9 shows the transition velocity of each test with error bias. From this figure, the threshold velocity is  $26.4 \text{ m/s} \pm 2.0 \text{ m/s}$ .

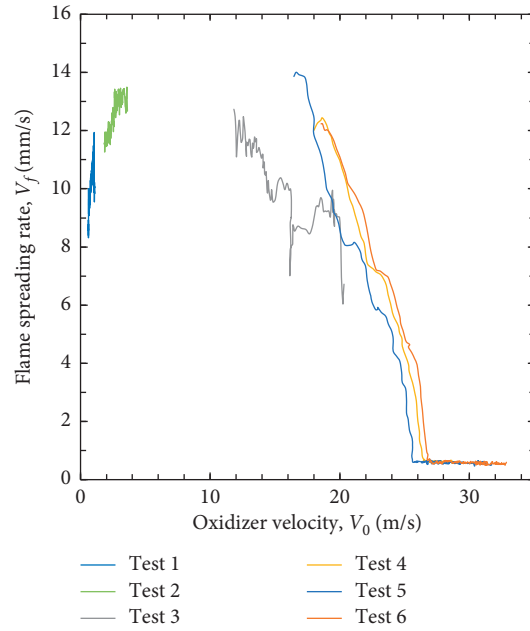


FIGURE 6: Flame spreading rate vs. oxidizer flow rate.

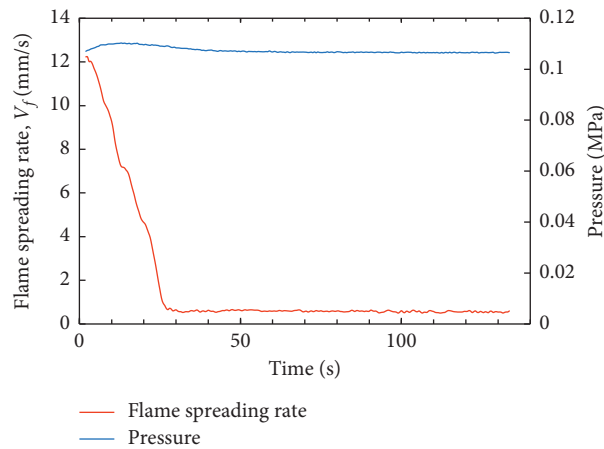


FIGURE 7: Pressure and flame spreading rate histories (Test 6).

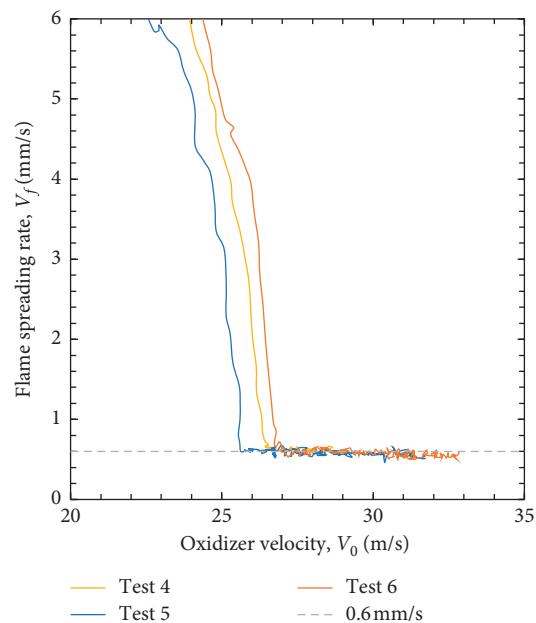


FIGURE 8: Flame spreading rate vs. oxidizer velocity near blow-off limit.

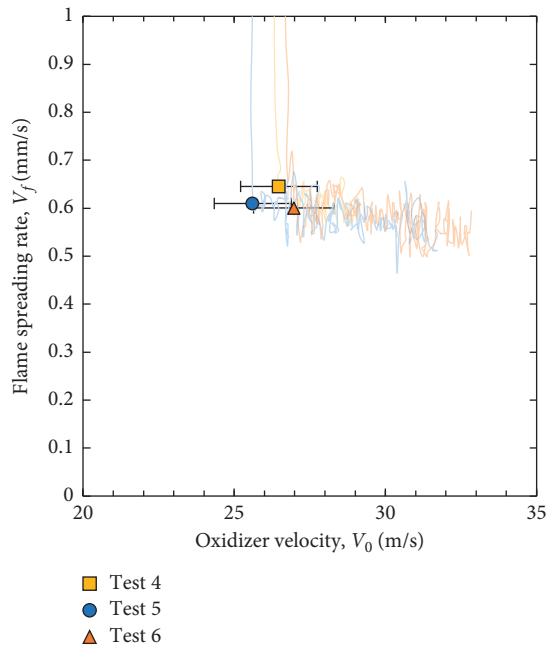


FIGURE 9: The threshold velocity with each error bias.

## 5. Conclusions

By using the expanding fuel duct, the continuous transition from flame spreading combustion to stabilized combustion was observed for the first time. The  $V_f$ - $V_o$  relation near the blow-off limit was also clarified. From several firing tests, it was found that a threshold oxidizer velocity of the transition can be determined. In this study, the threshold velocity was  $26.4 \text{ m/s} \pm 2.0 \text{ m/s}$ . This result is expected to be useful for the design of the Axial-Injection End-Burning Hybrid Rocket to prevent the backfiring problem.

## Data Availability

The data used to support the findings of this study are available from the corresponding author upon request.

## Conflicts of Interest

The authors declare that there are no conflicts of interest regarding the publication of this paper.

## Acknowledgments

This work was supported by the Hattori Hokkokai Foundation 17-006.

## References

- [1] I. S. Wichman, "Theory of opposed-flow feed," *Progress in Energy and Combustion Science*, vol. 18, no. 6, pp. 553–593, 1992.
- [2] N. Hashimoto, S. Watanabe, H. Nagata, T. Totani, and I. Kudo, "Opposed-flow flame spread in a circular duct of a solid fuel: influence of channel height on spread rate," *Proceedings of the Combustion Institute*, vol. 29, no. 1, pp. 245–250, 2002.

- [3] N. Hasimoto, H. Nagata, T. Totani, and T. Kudo, "Determining factor for the blowoff limit of a flame spreading in an opposed turbulent flow, in a narrow solid-fuel duct," *Combustion and Flame*, vol. 147, no. 3, pp. 222–232, 2006.
- [4] T. Matsuoka, S. Murakami, and H. Nagata, "Transition characteristics of combustion modes for flame spread in solid fuel tube," *Combustion and Flame*, vol. 159, no. 7, pp. 2466–2473, 2012.
- [5] H. Nagata, H. Teraki, Y. Saito et al., "Verification firings of end-burning type hybrid rockets," *Journal of Propulsion and Power*, vol. 33, no. 6, pp. 1473–1477, 2017.
- [6] Y. Saito, T. Yokoi, H. Yasukochi et al., "Fuel regression characteristics of a novel axial-injection end-burning hybrid rocket," *Journal of Propulsion and Power*, vol. 34, no. 1, pp. 247–259, 2018.
- [7] Y. Saito, M. Kimino, A. Tsuji, Y. Okutani, K. Soeda, and H. Nagata, "High pressure fuel regression characteristics of axial-injection end-burning hybrid rockets," *Journal of Propulsion and Power*, vol. 35, no. 2, pp. 328–341, 2019.
- [8] S. Bhattacharjee, R. Ayala, K. Wakai, and S. Takahashi, "Opposed-flow flame spread in microgravity-theoretical prediction of spread rate and flammability map," *Proceedings of the Combustion Institute*, vol. 30, no. 2, pp. 2279–2286, 2005.
- [9] A. C. Fernandez-Pello, S. R. Ray, and I. Grassman, "Flame spread in an opposed forced flow: the effect of ambient oxygen concentration," *Symposium (International) on Combustion*, vol. 18, no. 1, pp. 579–589, 1981.